Am J Cancer Res 2023;13(8):3463-3481
www.ajcr.us /ISSN:2156-6976/ajcr0150976

Original Article

CircCRIM1 suppresses osteosarcoma progression via sponging miR146a-5p and targeting NUMB

Jinnan Chen[1*], Ruoxuan Hei[1,2*], Chen Chen[1], Xuan Wu[1], Tiaotiao Han[1], Huiqin Bian[1], Junxia Gu[1], Yaojuan Lu[1,3], Qiping Zheng[1,3]

[1]*Department of Hematological Laboratory Science, Jiangsu Key Laboratory of Medical Science and Laboratory Medicine, School of Medicine, Jiangsu University, Zhenjiang 212013, Jiangsu, China;* [2]*Department of Clinical Diagnose, Tangdu Hospital, Air Force Medical University, Xi'an 710000, Shaanxi, China;* [3]*Shenzhen Walgenron Bio-Pharm Co., Ltd., Shenzhen 518118, Guangdong, China.* [*]*Equal contributors.*

Received April 29, 2023; Accepted May 26, 2023; Epub August 15, 2023; Published August 30, 2023

Abstract: CircCRIM1 (hsa_circ_0002346) is a circular RNA derived from gene *CRIM1* (the cysteine rich transmembrane BMP regulator 1 circRNAs) by back-splicing. Recent studies have suggested the diverse function of CircCRIM1 in the tumorigenesis of multiple malignancies, including osteosarcoma (OS). Here, we investigated the role and mechanism of circCRIM1 during OS progression. Differentially expressed circRNAs (including circCRIM1) in OS and human osteoblast (hFOB1.19) cell lines were selected by searching the circRNA expression microarray dataset of GSE96964. The expression levels of circCRIM1 and its sponging miRNAs and target genes were examined by RT-qPCR. The effects of circCRIM1 on the proliferation, migration, and invasion of OS cells were investigated by *in vitro* gain of function experiments. The *in vivo* function of circCRIM1 on OS was evaluated by measuring the subcutaneous and in situ tumor growth in nude mice. In addition, dual-luciferase reporter assay and in situ hybridization (FISH) were performed to explore the underlying mechanisms of circCRIM1 and its sponging miRNAs and target genes in OS. CircCRIM1 is downregulated in human OS cell lines and predominantly presents in the cytoplasm as demonstrated by RT-qPCR and FISH assays. Overexpression of circCRIM1 suppressed the migration, invasion, proliferation of OS cells *in vitro* and OS tumor growth *in vivo*. Mechanistically, we identified miR146a-5p as a sponge miRNA of circCRIM1 through bioinformatic prediction and confirmed their interaction and colocalization via reporter gene assay and FISH analysis. This interaction leads to increase expression of the downstream target gene NUMB, which will cause inhibition of the Notch signal pathway. We further demonstrated that miR146a-5p overexpression could reverse the antitumor effect induced by circCRIM1 in OS cells. Our results support that circCRIM1 acts as a tumor suppressor in OS by sponging miR146a-5p and its downstream target NUMB.

Keywords: Osteosarcoma, circular RNA, circCRIM1, miR146a-5p, NUMB

Introduction

Osteosarcoma (OS) is the most common primary bone malignant tumor typically occurs in adolescents (15-19 years old) with a maximum annual incidence of 8-11 per 10,000 [1, 2]. Currently, the mainstay treatment options for OS include limb-sparing surgery to remove the primary tumor, along with preoperative, and postoperative adjuvant chemotherapy [3-5]. However, given its high incidence of metastasis, the 5-year survival rate of OS remains low [6, 7]. Despite the presurgical systemic chemotherapy with postoperative adjuvant immunotherapy having greatly improved the treatment efficacy, the long-term survival rate for OS patients with pulmonary metastases is still less than 20% [8, 9]. This is possibly due to the fact that the etiology of OS is still not clear. Therefore, further understanding the pathological mechanism of OS will help with identification of its diagnostic markers and therapeutic targets and thus improve its survival.

Non-coding RNAs (ncRNAs) are RNA molecules that are not translated into protein products but may participate in multiple cellular processes and functions with their different classes of ncRNAs. Most of the circular RNAs (circRNAs) are ncRNAs that have been identified in recent

years through high-throughput sequencing technology. CircRNAs are a class of single-stranded closed-loop RNAs produced by a canonical back-splicing procedure and are widely expressed in a variety of eukaryotes. As other ncRNAs, circular RNAs have been shown to possess important regulatory functions via different mechanisms. For example, after ischemic stroke, circSCMH1 enhances vascular repair and motor function recovery via FTO-regulated m6A methylation, providing insights into the mechanism of circRNA in brain injury after acute ischemic stroke [10]. Yuan et al. [11] reported that in Diabetic cardiomyopathy (DCM), circRNA mm9_circ_008009 could rescue the cardiomyocytes pyroptosis by binding with valosin-containing protein (VCP) and blocking of the Med 12 protein degradation.

Several research studies have found that circRNA is not only involved in the regulation of various physiological activities, but also participates in the occurrence and development of tumorigenesis from many aspects [12-15]. In melanoma, downregulated circZNF609 inhibited melanoma metastasis through binding with FMRP to inhibit the RAS-related C3 botulinum toxin substrate 1 [16]. Likewise, circular RNA cSERPINE2, which was significantly elevated in breast cancer, showed a positive correlation with poor clinical outcomes. Circular RNA cSERPINE2 was able to enhance Interleukin-6 (IL-6) secretion by tumor-associated macrophages (TAMs) and promote the proliferation and invasive ability of breast cancer cells [17].

CircCRIM1 was derived from the cysteine rich transmembrane BMP regulator 1 (CRIM1) by back-splicing [18]. In addition, circCRIM1 is involved in the progression of several cancers [19-22]. For example, circCRIM1 was elevated both in highly metastatic nasopharyngeal carcinoma (NPC) cells and NPC tissues with distant metastasis, overexpression of circCRIM1 competitively bound to miR-422a and suppress the inhibitory effect on the target gene FOXQ1, ultimately promoting in metastasis and docetaxel chemoresistance and Epithelial-Mesenchymal Transition (EMT) of NPC cells [23]. Furthermore, recent studies suggest circCRIM1 acts as a tumor suppressor in non-small cell lung cancer (NSCLC). CircCRIM1 suppressed the immune evasion of NSCLC via destabilized HLA-F mRNA via competing interaction with IGF2BP1 [24]. Interestingly, two studies have reported that circCRIM1 exerts diametrically opposed biological effects in OS cell lines, through a ceRNA mechanism, Liu et al. found that knockdown of circCRIM1 (circ_0053958) facilitates the autophagy of OS cells through inhibits the histone deacetylase 4 (HDAC4), which is a subunit of class II histone deacetylases, to impede the progression of OS. Another group of researchers proposes that circCRIM1 inhibits OS progression at the cellular level [25, 26]. Nevertheless, the specific role and mechanism of circCRIM1 *in vivo* is remain elusive, and exploration of circCRIM1 cannot fully accounted the diversity of its involvement in OS progression. Therefore, there is an urgent need to elucidate the functions of circRNAs derived from CRIM1.

Methods

Cell culture and treatment

HEK-293T, human osteoblast hFOB1.19 and human osteosarcoma cell lines including MNNG/HOS, MG63, and U2OS were obtained from the Cell and Stem Cell Bank, Chinese Academy of Sciences (Shanghai, China). 143B were purchased from FuHeng Biology (Shanghai, China). HEK-293T, MNNG/HOS, and MG63 were cultivated in DMEM (Gibco, Carlsbad, CA, USA) with 10% fetal bovine serum (FBS); U2OS and 143B cells were cultured in McCoy's 5 and RPMI-1640 medium (Biological Industries, USA) with 10% fetal bovine serum (FBS) respectively. hFOB1.19 cells were fostered in DMEM/F12 (1:1) (Biological Industries, USA) supplemented with 10% FBS. All the cells were cultured in a cell incubator at 37°C with 5% CO_2 and supplemented with 100 U/mL of penicillin (Biosharp life science, China) and 100 μg/ml streptomycin (Biosharp life science, China).

RNA extraction and RT-qPCR

Total RNA was isolated from cells with TRIzol® reagent (Invitrogen, Thermo Fisher Scientific, Inc., USA) following the manufacturer's instruction. After spectrophotometric quantification, 1 μg of total RNA in a final volume of 20 μL was used for reverse transcription (RT) with a PrimeScript™ RT reagent Kit with gDNA Eraser (Perfect Real Time) (TaKaRa, Japan). To examine the gene expression level of circRNA and

Table 1. Primers for RT-qPCR and miRNA fragment

List of oligonucleotide sequences	
Gene	Sequence (5'-3')
circCRIM1-Divergent-Forward	CCCGGACAGCTATGAAACTC
circCRIM1-Divergent-Reverse	GCAGCCAGCAATAAGGTTTT
circCRIM1-Convergent-Forward	CCGCTGTGAAGTCCAGTTCT
circCRIM1-Convergent-Forward	CTGGGTAAGGGACAGCACTC
CRIM1-Forward	GGTTCCTGTTGTGCTCTTGT
CRIM1-Reverse	TGCCAAGAATCAAGTTGCAGATAA
β-actin-Forward	GCATGGGTCAGAAGGATTCC
β-actin-Reverse	AGGATGCCTCTCTTGCTCTG
U6-Forward	CTCGCTTCGGCAGCACA
U6-Reverse	AACGCTTCACGAATTTGCGT'
NUMB-Forward	AGGCCAGTCGTCCACATCA
NUMB-Reverse	GGTACTTAACCGGGAAGCTACAT
miRNA fragment	
Mimic NC	5' UUUGUACUACACAAAAGUACUG 3'
Mimic NC	3' AAACAUGAUGUGUUUUACUGAC 5'
miR-146a-5p mimic	5' UGAGAACUGAAUUCCAUGGGUU 3'
miR-146a-5p mimic	3' ACUCUUGACUUAAGGUACCCAA 5'
Inhibitor NC	5' CAGUACUUUUGUGUAGUACAAA 3'
miR-146a-5p inhibitor	5' ACUCUUGACUUAAGGUACCCAA 3'
FISH Probe	
Cy3-circCRIM1	TCATCAGTCCAGT+TCTCATCTTG+TTGGCAAAGTACAGC
Fam-miR146a-5p	AACCCATGGA ATTCAGTTCT CA

mRNA, reverse transcription quantitative real-time PCR (RT-qPCR) was performed with ultra-SYBR Premix (CWBIO, China) by the Applied Biosystems QuantStudio 5 PCR instrument (ThermoFisher Scientific, USA) according to the thermocycling conditions respectively. β-actin was used as an internal control of circRNA and mRNA, and U6 was used for miRNA. The $2^{-\Delta\Delta Ct}$ method was used to calculate the fold change of the target genes. Further detail of primer sequences used in our study was shown in **Table 1**.

Plasmid construction, miRNA transfection, and lentiviral infection

The overexpression plasmid of circCRIM1 (pLC5-ciR-CRIM1) was constructed by Geneseed Ltd. (Guangzhou, China) while the empty plasmid (pLC5-ciR-NC) was used as a negative control. microRNA mimics and inhibitors were designed and purchased from RiboBio (Guangzhou, China) and transfected into cells via Lipofectamine 3000 reagent (Invitrogen, Carlsbad, CA, USA) according to the manufacturer's instruction with a final concentration at 50 nM. The circCRIM1-overexpression lentivirus synthesized by Obio Technology Corp., Ltd. (Shanghai, China) was used to establish stable transfectants. The stable cell lines were screened by culturing in the medium containing 5 μg/mL puromycin (Sigma, USA). The transfection efficiency was confirmed by RT-qPCR. All the sequences of microRNA mimics and inhibitors used in this study were listed in **Table 1**.

Western blot analysis and antibodies

Total cellular protein was extracted with radioimmunoprecipitation assay buffer (RIPA, Beyotime, China) supplemented with 1× PMSF (Beyotime, China), and the supernatant was collected and quantified by spectrophotometer. An equal amount of protein extracts (100 μL) was separated by 10% SDS-PAGE gel at 100 V for 1.5-2 hours then transferred to the 0.22 μm PVDF membrane (Millipore, Billerica, MA, USA) at 350 mA for 90 mins. The membranes were incubated with specific primary antibodies at

4°C overnight after blocking at 5% fat-free milk for 2 hours at room temperature. The next day, after washing the membrane three times with 1× TBST for 15 mins, the membrane was incubated with the corroding HRP-labelled secondary antibodies for 1 hour at room temperature. Finally, the target bands were visualized by chemiluminescence using a GE Amersham Imager 600. The detail of antibodies was: NUMB (1:500, HUABio, JM10-023); β-actin (1:2000, Beyotime Biotechnology, AF0003); NOTCH1 (1:1000, SAB, #30991); HES-1 (1:1000; Abcam, ab71559) in primary antibody dilution (Yeasen Biotechnology, China).

Nuclear and cytoplasmic extraction

The nuclear and cytoplasmic RNAs were extracted from MNNG/HOS and MG63 cells with the PARIS™ Kit (Life Technologies, Austin, Texas, USA) following the manufacturer's protocols. Briefly, Cell Fraction Buffer was used to resuspend cells and incubate the mixture on ice for 15 mins, the mixture will then divide into two parts after centrifuging for 5 mins at 500 RPM at 4°C. The supernatant was transferred as the cytoplasmic fraction while the precipitate was washed with Cell Fraction Buffer and taken as part of the nuclear fraction.

RNase R and nucleic acid electrophoresis

For the RNase R treatment, we collected 10 μg of total cellular RNA and incubated with or without 3 U/μg RNase R (Geneseed biotechnology, Guangzhou, China) for 15 mins at 37°C water baths. The digested product was further subjected to the subsequent RT-qPCR. The PCR outgrowth was implemented in Nucleic acid electrophoresis, the gDNA and cDNA were separated with 2% agarose gel electrophoresis with 1× TAE buffer. DNA was separated by electrophoresis at 120 V for 30 mins. The TaKaRa DNA marker (TaKaRa, TDL500, 3590A) was used to indicate the position. The bands were detected by ultraviolet radiation.

Fluorescence in situ hybridization (FISH)

SA-Cy3-labeled circCRIM1 probes and SA-FAM labeled miR146a-5p probe were designed and synthesized by GenePharma (Shanghai, China), and the sequences are available in **Table 1**. U2OS and MNNG/HOS cells were planted onto the proprietary coverslips of a confocal microscope for 24 hours, after being fixed with 4% paraformaldehyde, the cells were incubated with 1% circCRIM1 probe working solution overnight in the 37°C incubators away from light. Nuclei were counterstained with DAPI for 1 hour before collecting the photography. The signal of the probe was detected and magnified by Fluorescence in Situ Hybridization Kit (GenePharma, Shanghai, China). These images were taken under a Leica Confocal Laser Scanning Microscope (CLSM) (Wetzlar, Germany).

5-ethynyl-20-deoxyuridine (EdU assay)

The EdU assay was performed to confirm the proliferation ability of OS cells by using the Cell-Light EdU Apollo567 In Vitro Kit (RiboBio, Guangzhou, China). Firstly, the cells were plated and cultured in 96-well plates for 24 hours, and then each well was incubated with 100 μL 50 μm EdU working solution for 2 hours at 37°C incubators. After being fixed with 4% paraformaldehyde, the cells were permeabilized with 0.5% Triton for 30 mins at room temperature and then sequentially stained darkly with 100 μL 1× Apollo® and 1× Hoechst 33342 on a shaker for 30 mins. The images were taken under the Olympus IX73 Inverted Microscope.

Transwell migration and Matrigel invasion assays

The migration assay was conducted by using the Transwell chamber (CORNING, USA). About 200 μL serum-free suspension of cells were added into the central part of the upper chamber (about 2-4×10^4 depending on the cells type, 4-8×10^4 for invasion assay). Meanwhile, 600 μL basal medium with 10% fetal bovine serum was put into the lower part of the chamber as a chemoattractant to induce cell migration to the other side. After 24 hours of incubation at 37°C, the transferred cells were fixed with 4% paraformaldehyde and subsequently stained with 1% crystal violet (Beyotime, Shanghai, China) for 30 mins respectively. For the invasion assay, the chamber was precoated with Matrigel (BD Science, Bedford, MA, USA) following the instruction of the manufacturer. The result of migration and invasion rates was counted and evaluated at least in three random fields.

Proliferation assay

Cell Counting Kit-8 (CCK8, Yeasen Biotechnology, China) was used to assess the prolifera-

tion ability of OS cells. The density of 4-6×10^3 cells was seeded into the 96-well plates and 10 μL CCK8 reagent plus 90 uL completely medium were mixed and added to each 5 duplicated wells at 0, 24, 48, and 72 hours after planting the cells. The absorbance values of optical density (OD) were measured at 450 nm by BioTek 800 TS absorbance reader. All experiments were repeated three times independently.

Colony formation assay

About 0.5-1×10^3 treated cells were cultured on 6-well plates per well for 14 days, and the medium was changed once during this period. After being washed twice with PBS and fixed with 4% paraformaldehyde, the colonies were stained with 1% crystal violet (Beyotime, Shanghai, China) for 30 mins. The images were taken by Canon EOS 700D.

Wound healing assay

After transfected circRNAs and miRNA, the OS cells were seeded on 6-well plates evenly, the cells monolayers were vertically scarped using 200 μL sterile pipette tips while the density of cells reaches 80% (regarded as 0 hour). Subsequently, each wound was captured every 24 hours. The relative migration ability was quantified according to the relative distance normalized to 0-hour control.

Dual-luciferase reporter assay

The wide-type and mutant plasmids (mut-circCRIM1; wide-type circCRIM1; NUMB; mut-NUMB) were constructed and inserted downstream of the luciferase reporter gene in the dual luciferase plasmid pmirGLO (RiboBio, Guangzhou, China). HEK-293T cells were seeded on 24-well plates and were co-transfected with the plasmid and miRNA mimics or NC (RiboBio, Guangzhou, China) by using Lipofectamine 3000 (Invitrogen, Carlsbad, CA, USA) while cell reaches 40% confluence. After 48 hours the Dual-Luciferase reporter assay kit (Promega E1901, Madison, WI, USA) was employed to measure the activities of firefly and Renilla luciferase.

Subcutaneous and orthotopic xenograft tumor models

All animal experiments were approved by the Ethics Committee of Jiangsu University. For the xenograft tumor model assays, 4-5-week-old male BALB/c nude mice provided by Gem Pharmatech Co., Ltd. (Nanjing, China) were randomly divided into 4 groups (n = 6 for each group), and 5×10^6 cells of MNNG/HOS cell line that stably over-express circCRIM1 and undergo logarithmic growth were collected to construct the xenograft tumor models. Briefly, the cells were trypsinized, counted, and resuspended in the precooled Phosphate-Buffered Saline. Subsequently, 100 μL of suspensions were injected into the right dorsal abdomen of mice subcutaneously, while the orthotopic tumor models were injected into the upper tibial mid-tibial of the right hind limb. After 4-5 weeks post-injection, mice were executed to collect the tumor tissue and weighed, and then fixed with 4% paraformaldehyde for following H&E staining and histology analysis.

Histology and immunohistochemistry (IHC)

IHC staining was performed to detect the expression level of target gene in situ. Briefly, the xenograft tumor tissues were collected and fixed with 4% paraformaldehyde solution for 24 hours then dehydrated in ethanol, embedded in paraffin, and cut into 5 μm sections. After being dewaxed with xylene and rehydrated with a gradient of ethanol, the slides were incubated with 100 μL primary antibody overnight in the humidified chamber (4°C), then incubated with secondary antibody at room temperature for 1 hour after washing the slides with 1× TBST three times. Finally, the slides were stained with freshly prepared DAB substrate until suitable staining develops. The images of slides were observed and captured by Nikon ECLIPSE E200. The antibodies used were for NUMB (1:80, HUABio, JM10-023); NOTCH1 (1:150, SAB, #30991); HES-1 (1:1000; Abcam, ab71559).

Bioinformation prediction

The data of differentially expressed circRNAs were accessed from the microarray expression database GSE96964 from the GEO database (https://www.ncbi.nlm.nih.gov/gds), in which information is freely available online. We used ArrayStar human circRNA Array to obtain microarray-based circRNA expression profiles. Further, we used R studio to compare the sequences of all circRNAs within the dataset with known human circRNA sequences in cir-

cBase for ID conversion to obtain information on differentially expressed circRNAs. In the process of implementing ID conversions, we use R package 'data.table', while all the code that we used and original documents are provided in the Supplementary Materials 1, 2, 3 and 4.

To analyze the mechanism of circRNAs exercised in OS, we used bioinformatic databases Circbank (http://www.circbank.cn/), miRanda (http://www.microrna.org), RNAHybird (http://bibiserv.techfak.uni-bielefeld.de/rnahybrid/), and ENCOR (ENCORI: The Encyclopedia of RNA Interactomes. (sysu.edu.cn)) to across-analysis the overlapping miRNA that may bind to circCRIM1. Filtering restrictions were complied as follows: (i) Total score ≥ 140 and Total energy < 4 kcal/mol; (ii) Number of estimated binding sites > 1; and (iii) Minimum free energy (MFE) ≤ 0 kcal/mol.

To further explore the potential mechanism associated with miR146a-5p mediated regulation of OS, we performed another bioinformatic analysis using the online programs TargetScan Human 8.0 (https://www.targetscan.org/vert_80/), miRTargetLink (https://ccb-web.cs.uni-saarland.de/mirtargetlink/), miRPathDB 2.0 (https://mpd.bioinf.uni-sb.de/) and starbase-ENCOR (ENCORI: The Encyclopedia of RNA Interactomes. (sysu.edu.cn)).

Statistical analyses

Quantitative data were expressed as mean ± SEM (standard error of the mean), and the statistical analysis was conducted using GraphPad Prism 8.0 (GraphPad Software, La Jolla, USA). Differences between the means of two groups were analyzed by Student's t-test, while one-way ANOVA was performed between multiple groups. Data were obtained from at least three independent experiments and $P < 0.05$ was considered statistically significant.

Result

CircCRIM1 is downregulated in human OS cell lines and is predominantly localized in the cytoplasm

To investigate how circRNA may play a role in OS, we searched the GEO database for OS microarray sets to screen for differentially expressed circRNAs and the non-coding RNA profiling GSE96964 was selected for this study [27]. The absolute value of fold-change ≥ 1.5 and *P*-value < 0.05 were set as the screening criteria to sort the raw data, and then plotted with the heat map. We obtained 81 differentially expressed circRNAs with 17 up-regulated and 64 down-regulated (**Figure 1A**). The basic information of the twelve circRNAs that were most significantly up- or down-regulated were as tabulated (**Figure 1B**). Hsa_circ_0002346 was one of the most down-regulated circRNAs. We further demonstrated that hsa_circ_0002346 (chr2: 36623756-36,669,878) was formed by circularization of exons 2, 3, and 4 of the *CRIM1* gene locus (chromosome 2p22.2), and thus named circCRIM1_021 according to the circRNA ID in circBase (http://circbase.org/cgi-bin/simplesearch.cgi). Sanger sequencing confirmed the back-splicing junction products as shown by RT-qPCR amplification using the specific divergent primers (**Figure 1D**).

We then examined the expression level of circCRIM1 in OS cell lines, and in agreement with the GEO database, circCRIM1 was significantly downregulated compared to human osteoblasts cell line h. FOB1.19 (**Figure 1C**), We have utilized RNase R digestion assay to examine the stability of the special stem-loop structure of circRNA, in total RNA from MNNG/HOS and MG63 cells [28, 29], and the results showed that RNase R was able to significantly attenuate the content of linear CRIM1 (blue arrow), while there was no significant change in circCRIM1 (red arrow) (**Figure 1E-G**). Additionally, to further investigate the distribution of circCRIM1, nucleoplasmic separation experiments and FISH assays were performed, and the results support that circCRIM1 was mostly localized in the cytoplasm (**Figure 1H**, **1I**).

CircCRIM1 inhibits the migration, invasion and proliferation of OS cells

To evaluate the potential role of circCRIM1 in OS, we successfully constructed and overexpressed circCRIM1 (pLC5-ciR-CRIM1) in OS cell lines by transfection. The data showed that the plasmid accurately and efficiently cyclized circCRIM1 without elevating the level of linear CRIM1 in OS cell lines (**Figure 2A**). The colony formation, cck-8 and EDU assays revealed that circCRIM1 predominantly inhibited the proliferation capacity of OS cell lines (**Figure 2B-G**).

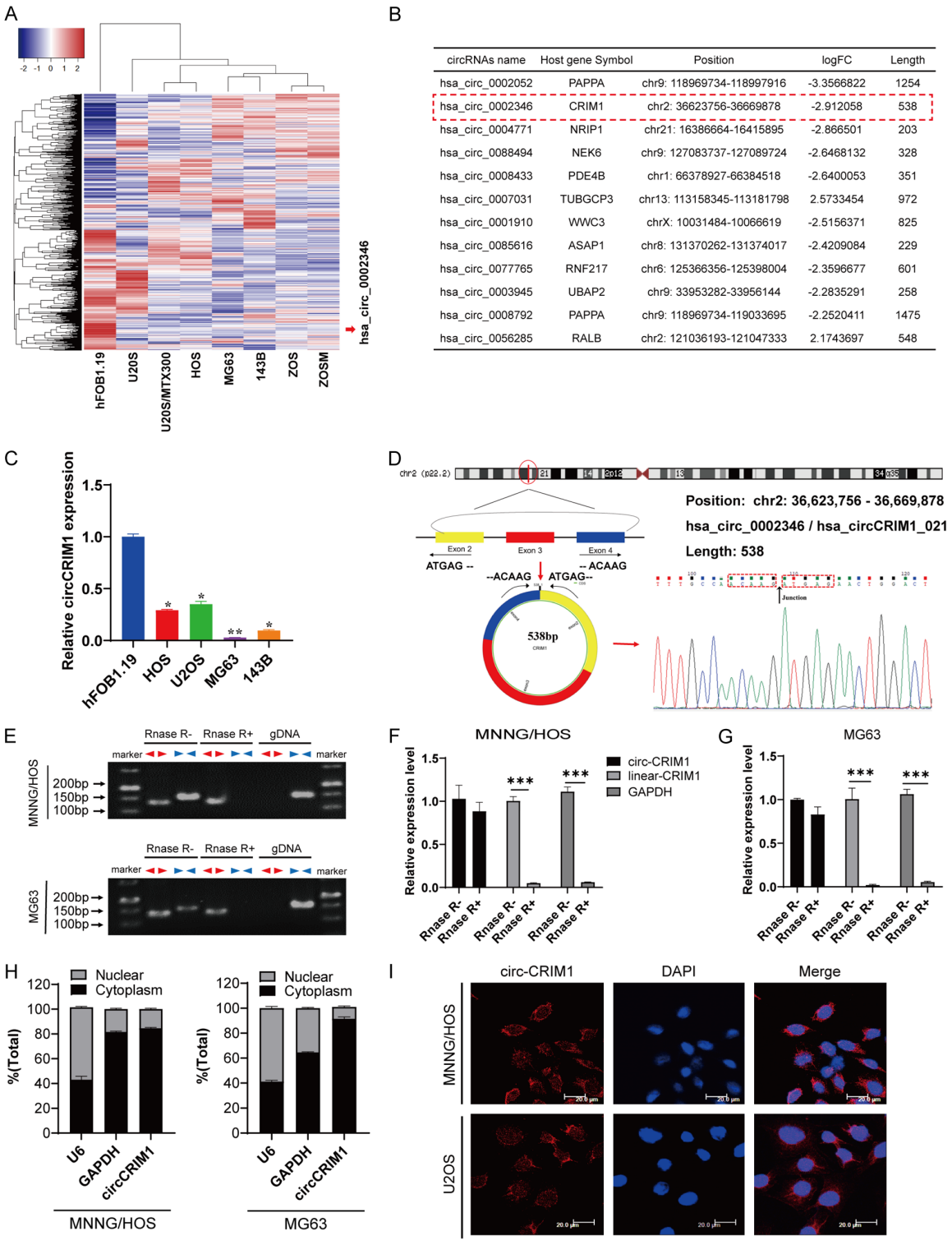

circRNAs name	Host gene Symbol	Position	logFC	Length
hsa_circ_0002052	PAPPA	chr9: 118969734-118997916	-3.3566822	1254
hsa_circ_0002346	CRIM1	chr2: 36623756-36669878	-2.912058	538
hsa_circ_0004771	NRIP1	chr21: 16386664-16415895	-2.866501	203
hsa_circ_0088494	NEK6	chr9: 127083737-127089724	-2.6468132	328
hsa_circ_0008433	PDE4B	chr1: 66378927-66384518	-2.6400053	351
hsa_circ_0007031	TUBGCP3	chr13: 113158345-113181798	2.5733454	972
hsa_circ_0001910	WWC3	chrX: 10031484-10066619	-2.5156371	825
hsa_circ_0085616	ASAP1	chr8: 131370262-131374017	-2.4209084	229
hsa_circ_0077765	RNF217	chr6: 125366356-125398004	-2.3596677	601
hsa_circ_0003945	UBAP2	chr9: 33953282-33956144	-2.2835291	258
hsa_circ_0008792	PAPPA	chr9: 118969734-119033695	-2.2520411	1475
hsa_circ_0056285	RALB	chr2: 121036193-121047333	2.1743697	548

Figure 1. Screening and validation of hsa_circ_0002346 in OS cell lines. A. The heatmap shows that there are 17 upregulated and 64 downregulated circRNAs in 7 human OS cell lines relative to matched human osteoblast cells. B. By querying in circBank, we list the basic information of the top 12 circRNAs with the most significant expression differences. C. The relative expression level of circCRIM1 in 4 OS cells was detected by RT-qPCR. D. Schematic illustration showing the generation of circCRIM1 via the circularization of exons 2 and 4 in CRIM1 (the red arrow), while the back-splice junction sequences were validated by Sanger sequencing. The red rectangle and black arrow indicated the head to tail splicing site. E. Agarose gel electrophoresis assay was performed to show the expression of circCRIM1 and linear CRIM1 mRNA in MNNG/HOS and MG63 cells after treating with or without the RNase R. The red arrow represents the circ-CRIM1, and blue arrows represents the linear-CRIM1. F, G. RT-qPCR was assessed to

verify the stability of circCRIM1 after RNase R treatment. H. Nuclear-cytoplasmic fractionation assay demonstrated that circCRIM1 was mainly located in the cytoplasm of MNNG/HOS and MG63 cells. I. RNA fluorescence in situ hybridization (FISH) in MNNG/HOS and U2OS cells further revealed the presence of circCRIM1 predominantly existed in the cytoplasm. The nuclear was stained with DAPI (blue fluorescence), and the circCRIM1 probes were labeled with SA-Cy3 (red fluorescence). The scan bar = 20 μm.

Moreover, the migration and invasion ability of OS cells was remarkably reduced after transient transfection with circCRIM1 expression plasmid (**Figure 2H-K**). In addition, the result of the 48 h wound healing assay demonstrated that circCRIM1 can attenuate the migration ability of OS cells (**Figure 2L-O**). Together, these data suggest that circCRIM1 functionally inhibits the proliferation and viability of OS cells *in vitro.*

CircCRIM1 acts as a sponge for miR146a-5p in vitro

Previous studies have suggested that circRNAs may act as a sponge for miRNAs so as to influence their target mRNAs and thus their biological functions [30-32]. Through searching the four miRNA target databases (miRanda, RNAHybrid, circBank, ENCORI) with the full-length sequence of circCRIM1, we identified three candidate miRNAs that could potentially bind to circCRIM1 (**Figure 3A**) [33-36]. Subsequently, we designed and synthesized stem-loop primers for three miRNAs separately to detect their expression levels in four OS cell lines transfected with circCRIM1 expression plasmid. RT-qPCR results show that miR146a-5p was stably and lowly expressed in four OS cell lines with over-expression of circCRIM1 (**Figure 3B**). Next, dual-luciferase reporter assays were conducted to verify the specific binding between miR146a-5p and circCRIM1. Through in silico analysis of the miRanda database, we found two potential sites on the circCRIM1 sequence that could bind with miR146a-5p (**Figure 3C**). The reporter plasmids were constructed with the sequences containing two mutant sites and wild-type circCRIM1 inserted downstream of the luciferase reporter gene. The relative luciferase activity in HEK-293T cells showed a significant reduction when the circCRIM1-WT reporter was co-transfected with miR146a-5p mimics. Mimics NC or miR146a-5p mimics showed no obvious difference when co-transfected with circCRIM1-WT or circCRIM1-MUT reporter (**Figure 3D**). In addition, miR146a-5p was prominently upregulated in 143B and MNNG/HOS cells than in human osteoblasts hFOB1.19 (**Figure 3E**). Finally, the FISH assay conducted in 143B cells and MNNG/HOS cells revealed that miR146a-5p were mainly concentrated in cytoplasm and co-localized with circCRIM1 (**Figure 3F**).

Enhancing miR146a-5p reverse the circCRIM1-induced antitumor effect in OS cells

miR146a has been implicated roles in the regulation of the immune and mainly the innate immune system, as well as in the regulation of chronic immune responses in the tumor microenvironment, such as the “dual role” of miR146a in breast cancer and colorectal cancer [37, 38]. To further elaborate on whether circCRIM1 plays a role in OS via competitive sponging of miR146a-5p, we designed several rescue experiments incorporating miR146a-5p. The Transwell migration assays and Matrigel invasion assays (**Figure 4A-D**) showed that the motility ability inhibited by circCRIM1 could be partially alleviated by miR146a-5p. Similar results were observed in the wound healing assays (**Figure 4E-H**). Meanwhile, in EDU assays (**Figure 4I-L**) and plate colony formation assays (**Figure 4M**, **4N**), we observed significant inhibition of proliferation capability of the cells over-expressing circCRIM1 but with exogenous upregulation of miR146a-5p expression. Collectively, these data suggest that circCRIM1 inhibits OS proliferation and migration through adsorption of miR146a-5p.

NUMB is downstream of miR146a-5p in OS cells

miRNAs are known to regulate tumor proliferation and growth by binding to the 3’UTR region of their downstream target genes. To elucidate the mechanism of miR146a-5p on OS, we successfully overexpressed and knocked down miR146a-5p in OS cell lines respectively via specific mimics and inhibitors (**Figure 5A**). Then, we performed the bioinformatics analysis of the four miRNA databases (TargetScan, miRTargetLink, miRPathDB, starbase ENCORI) and obtained 14 candidate target genes by per-

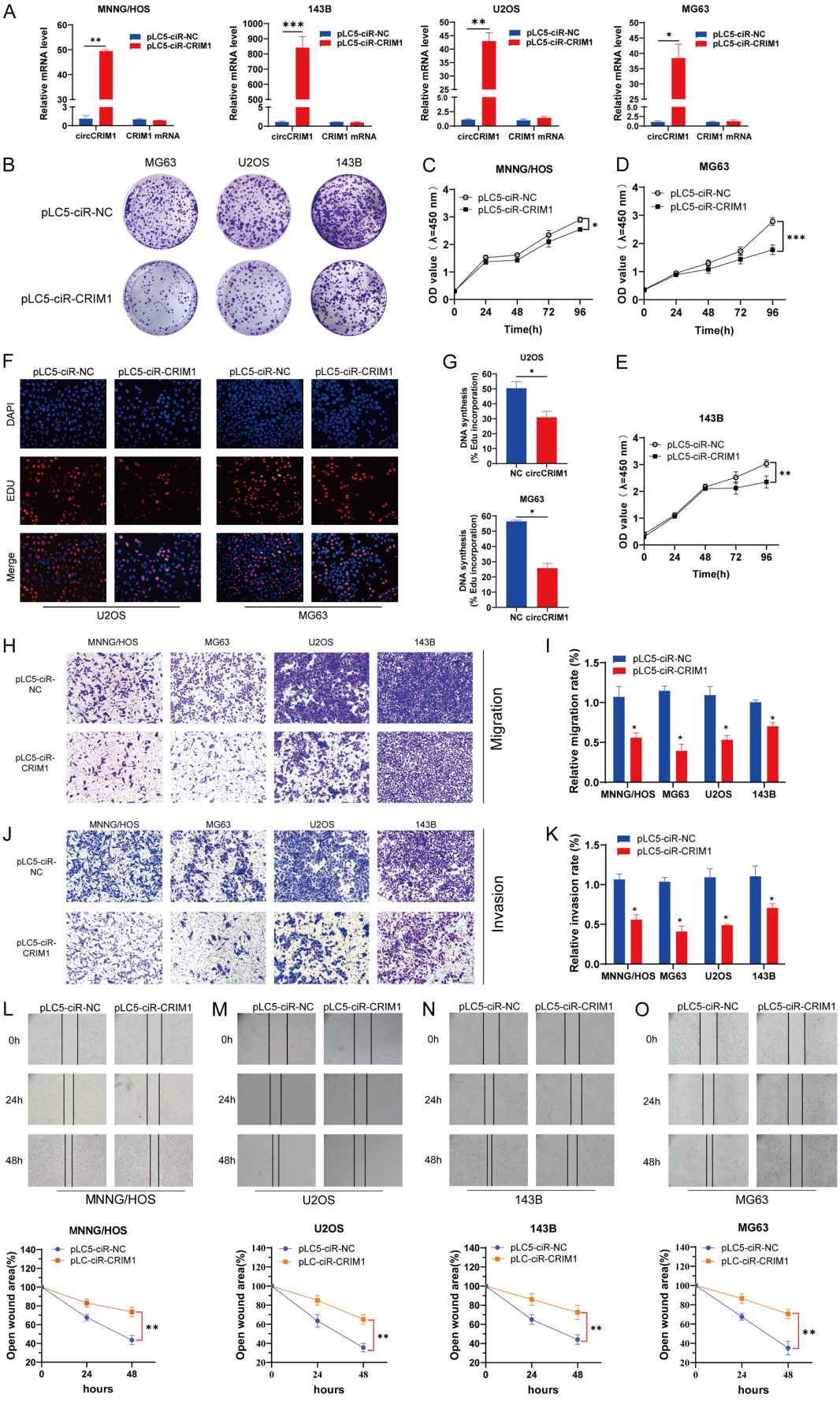
A
MNNG/HOS
143B
U2OS
MG63
Relative mRNA level
pLC5-ciR-NC
pLC5-ciR-CRIM1
circCRIM1
CRIM1 mRNA
B
MG63
U2OS
143B
pLC5-ciR-NC
pLC5-ciR-CRIM1
C
MNNG/HOS
D
MG63
OD value（λ=450 nm）
Time(h)
F
DAPI
EDU
Merge
U2OS
MG63
G
DNA synthesis (% Edu incorporation)
NC circCRIM1
E
143B
H
MNNG/HOS
MG63
U2OS
143B
Migration
I
Relative migration rate (%)
J
Invasion
K
Relative invasion rate (%)
L
M
N
O
0h
24h
48h
Open wound area(%)
hours

Figure 2. CircCRIM1 affects the migration, invasion and proliferation ability of OS cells. A. The expression level of circCRIM1 and CRIM1 mRNA in OS cells after being transfected with pLC5-ciR-CRIM1 plasmid and pLC5-ciR-NC (control plasmids) were detected by RT-qPCR. B. Colony formation assay was conducted after instantly transfected with pLC5-ciR-CRIM1 plasmid. C-E. The cell viability was assessed by CCK8 assay. F, G. EdU assay of U2OS and MG63 cells were performed to evaluate the proliferation ability. The sample was imaged at 200X magnification and scan bar = 100 μm. H, I. The migration ability of OS cells after over-expression circCRIM1 was assessed by Transwell assay. J, K. The invasion ability of OS cells after over-expression circCRIM1 was detected by Matrigel invasion assays. L-O. The wound healing assay of OS cells showed the migration ability after over-expression of circCRIM1. Data are represented as mean ± SEM. $*P < 0.05$, $**P < 0.01$.

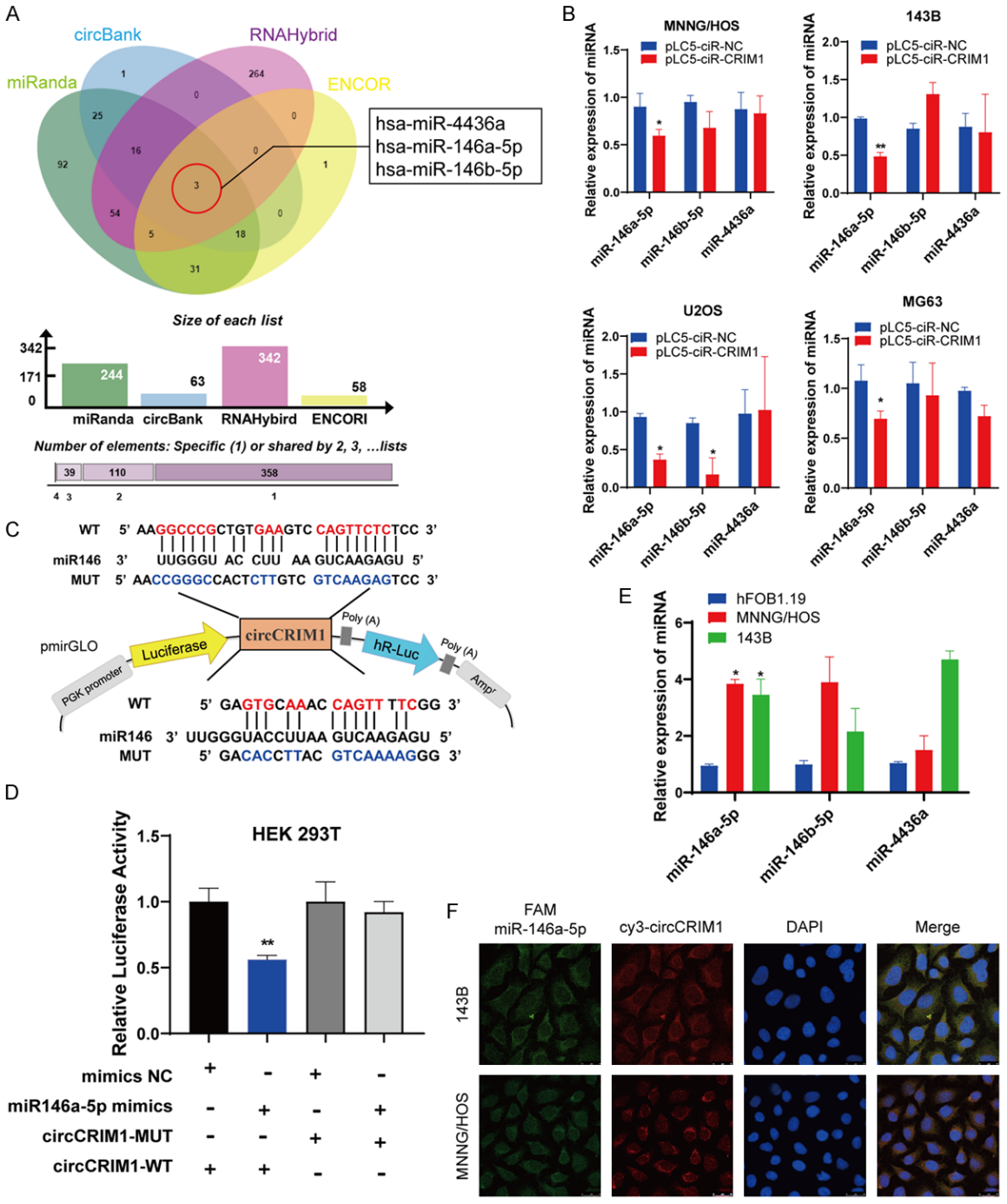

Figure 3. CircCRIM1 abundantly sponges miR146a-5p in OS cells. A. Overlapping region in the venny diagram shows the three microRNAs predicted by bioinformatics software that may bind to circCRIM1. B. The relative level of

predicted miRNAs after over-expression of circCRIM1 in osteosarcoma cells was assessed by RT-qPCR. C. The schematic illustrates the two binding seed sequences predicted by miRanda software and the mutant nucleotides of circCRIM1. D. The dual-luciferase reporter assay was conducted in HEK-293T cells by co-transfected with miR146a-5p mimics and wild-type circCRIM1 or mutant circCRIM1 plasmid. E. The basal expression level of microRNAs was detected in OS cells via RT-qPCR. F. The representative images of FISH displayed the SA-FAM labeled miR146a-5p (red fluorescence) which were co-localized with SA-cy3 labeled circCRIM1 (green fluorescence) mostly in the cytoplasm of 143B and MNNG/HOS cells. DAPI showed the nuclear and the magnification of images was 1000, Scan Bar = 25 μm. Data are represented as mean ± SEM. *$P < 0.05$, **$P < 0.01$.

forming sub-crossovers (**Figure 5B**) [39, 40]. The expression levels of these 14 candidate genes after being transfected with miR146a-5p mimics or inhibitors into MNNG/HOS, 143B, and MG63 cells were examined by RT-qPCR and the heat map was plotted coordinately (**Figure 5C**). **Figure 5D** shows the detailed changes of NUMB. We then selected seven of the genes with the most significant differences to examine their basal expression in human OS cell lines and osteoblast cell lines, and found that the NUMB gene, consistent with circCRIM1, was significantly downregulated in OS cells both at mRNA and protein levels (**Figure 5E**, **5F**). NUMB has been reported as a tumor suppressor in malignant tumors and negatively regulates the NOTCH signaling pathway [41]. Western blot results showed that transfection with miR146a-5p mimics led to down-regulation of NUMB and up-regulation of NOTCH and HES-1, whereas miR146a-5p inhibitors resulted in up-regulation of NUMB and decreased expression of NOTCH and HES-1 in OS cell lines MNNG/HOS and 143B cells (**Figure 5G**, **5H**).

We constructed the reporter plasmid containing the mutant and wild-type sites based on the complementary sequence predicted by TargetScan (**Figure 5I**). The reporter activity in HEK-293T cells was significantly decreased after co-transfection of miR146a-5p mimics with NUMB wild-type plasmids, but not in cells co-transfected with the mutant plasmids (**Figure 5J**). After confirming the direct binding effect of miR146a-5p to NUMB, we further investigated whether circCRIM1 could regulate the expression of NUMB and its downstream target NOTCH. The western blot results showed increased NUMB in MNNG/HOS and 143B cells after overexpression of circCRIM1, while NOTCH and HES-1 were downregulated (**Figure 5K**, **5L**). In addition, miR146a-5p and circCRIM1 co-transfection partially counteracted the downregulation of NUMB caused by miR146a-5p transfection alone and the upregulation of NUMB caused by overexpressing circCRIM1 alone. Similar results were also observed for NOTCH1 and HES-1 (**Figure 5M**, **5N**). Together, these results support that miR146a-5p directly binds with NUMB and controls the activity of NOTCH signaling and that circCRIM1 may inhibit the proliferation and migration of OS cells via the miR146a-5p/NUMB axis.

Over-expression of circCRIM1 suppresses tumorigenesis of xenograft tumors in vivo

To further determine whether circCRIM1 can serve as an inhibitor of tumor proliferation *in vivo*, we established heterotopic subcutaneous xenograft tumor as well as orthotopic xenograft tumor models in nude mice.

We constructed the lentiviral vector using the pLC5-ciR-CRIM1 plasmid, which successfully overexpressed circCRIM1 before. We validated the infection efficiency and assayed the expression levels of circCRIM1 in stable cell lines (**Figure 6A**, **6B**). Suspensions of MNNG/HOS cells stably transfected with circCRIM1 and negative control viruses (NC) were injected subcutaneously into the right abdominal back and the upper portion of the right tibial medullary cavity of 3-4-week-old male nude mice, respectively. Mice were sacrificed 4-5 weeks after the injection. The results showed that overexpression of circCRIM1 significantly reduced the volume and weight of tumors both subcutaneously (**Figure 6C**, **6D**) and orthotopically (**Figure 6E**, **6F**).

H&E staining of tumor tissue slides exhibited the morphology of each group of tumor cells. In the negative control group, neoplastic capillary infiltration was more obvious, and tumor cells were disorganized with large, displaced nuclei, deep staining, multiple nucleoli, and abnormal nuclei were common. The circCRIM1 overexpression group showed a moderate decrease in the number of tumor cells, more vacuoles in the tumor tissue, less common pathological nuclear fission, and less vascular infiltration.

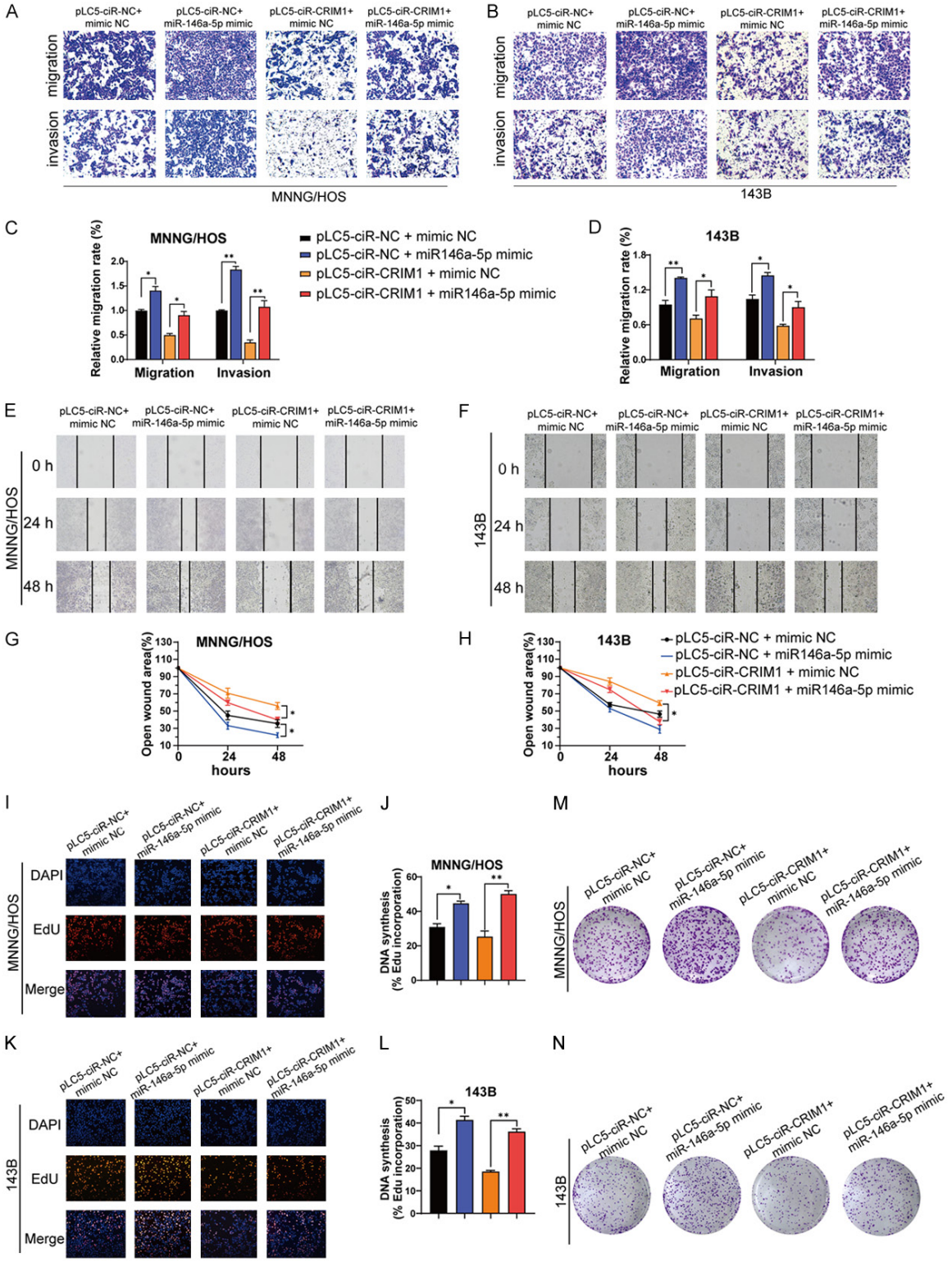

Figure 4. Over-expression of miR146a-5p reversed the circCRIM1 induced attenuation of cell proliferation, migration and invasion in OS cells. A-D. The transwell assay demonstrated the decreased migration and invasion ability induced by overexpressing circCRIM1 was rescued when co-transfected with miR146a-5p in MNNG/HOS and 143B cells. E-H. Co-transfected with miR146a-5p elevated the migration capacity of OS cells, which were suppressed while single transfected with circCRIM1, as determined by the wound healing assay. I-L. The EdU assay indicated that the proliferation ability of OS cells after overexpressing circCRIM1 was partially relieved by overexpressing miR146a-5p. M, N. The effect of circCRIM1 impeded on colony formation ability was ameliorated by co-transfected with miR146a-5p. Data are represented as mean ± SEM. $*P < 0.05$, $**P < 0.01$.

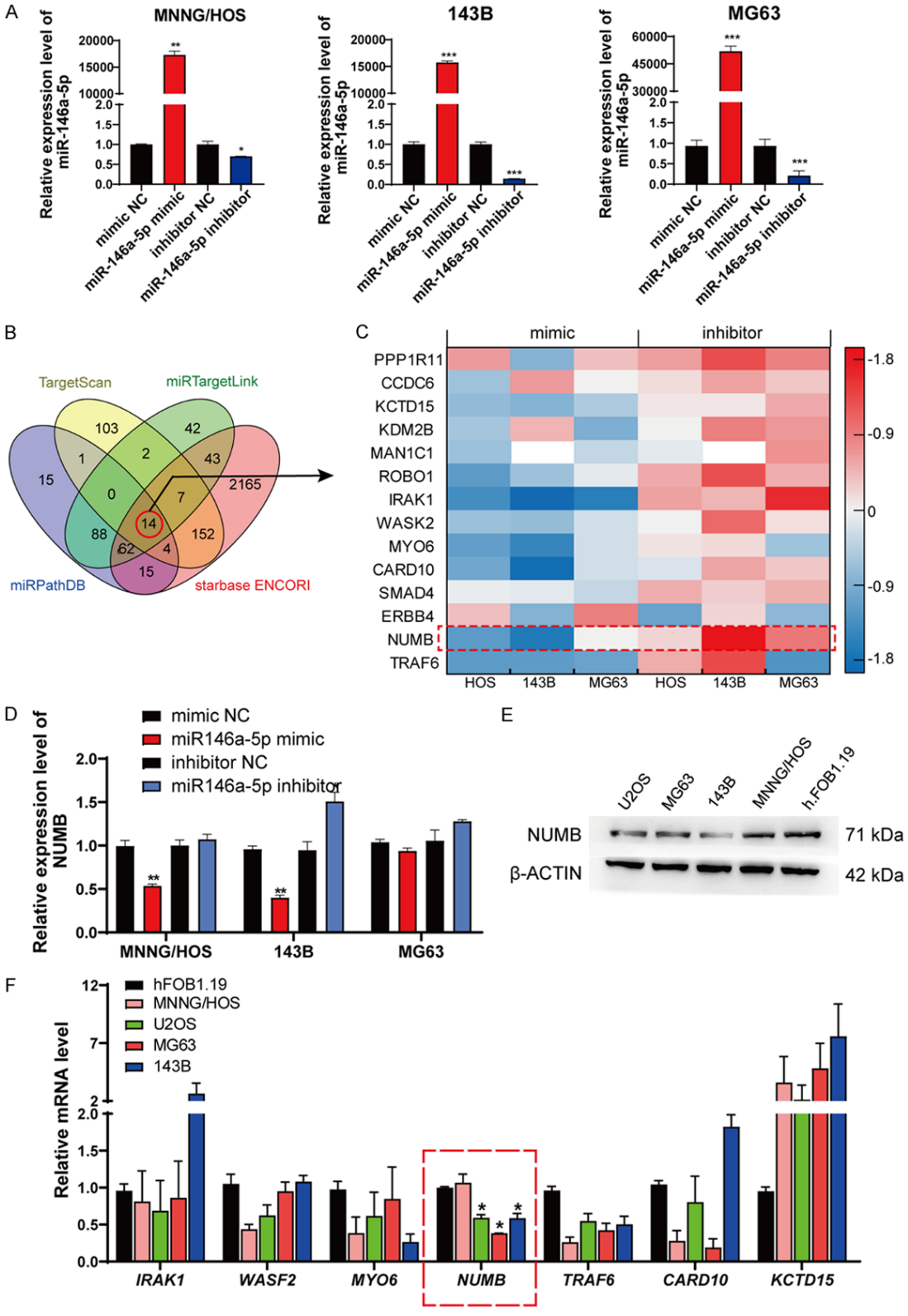
A
MNNG/HOS
143B
MG63
Relative expression level of miR-146a-5p
mimic NC
miR-146a-5p mimic
inhibitor NC
miR-146a-5p inhibitor
B
TargetScan
miRTargetLink
miRPathDB
starbase ENCORI
103
42
1
2
43
15
0
7
2165
14
88
152
62
4
15
C
mimic
inhibitor
PPP1R11
CCDC6
KCTD15
KDM2B
MAN1C1
ROBO1
IRAK1
WASK2
MYO6
CARD10
SMAD4
ERBB4
NUMB
TRAF6
HOS
143B
MG63
D
mimic NC
miR146a-5p mimic
inhibitor NC
miR146a-5p inhibitor
Relative expression level of NUMB
MNNG/HOS
143B
MG63
E
U2OS
MG63
143B
MNNG/HOS
h.FOB1.19
NUMB
β-ACTIN
71 kDa
42 kDa
F
hFOB1.19
MNNG/HOS
U2OS
MG63
143B
Relative mRNA level
IRAK1
WASF2
MYO6
NUMB
TRAF6
CARD10
KCTD15

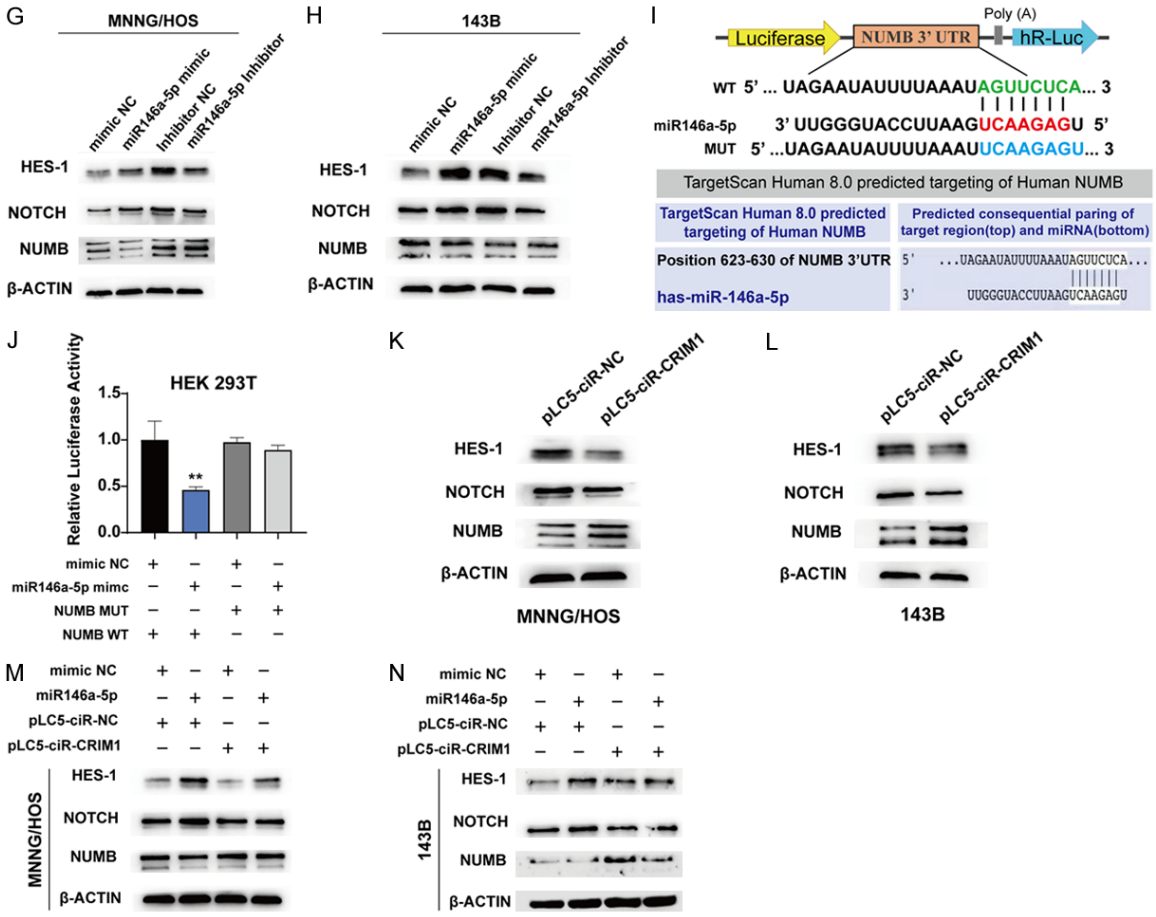

Figure 5. MiR146a-5p targets NUMB in OS cells. A. The relative expression of miR146a-5p after successfully transfected with mimics and inhibitors. B. Venny plots represent the 14 miR146a-5p downstream target genes predicted by TargetScan, miRPathDB, miRTargetLink and starbase ENCORI databases. C. The Cluster heatmap presents the expression of target genes after transfection with miR146a-5p mimics/inhibitors respectively. D. The specific fold changes in NUMB genes after exogenous effects on miR146-5p expression. E. The basal protein expression pattern of NUMB was assessed in OS cell lines compared with hFOB1.19 cells. F. The basal level of the above target genes in OS cells compared with hFOB1.19 were assessed. G. The protein expression level of NUMB in MNNG/HOS cells was downregulated by mimics and upregulated by inhibitors while NOTCH and Hes-1 were upregulated by mimics and downregulated by inhibitors (The middle band of NUMB represents the mainly expressed protein isoform in MNNG/HOS cells, which molecular was 71 kDa). H. The protein expression level of NUMB in 143B cells was downregulated by mimics and upregulated by inhibitors while NOTCH, Hes-1 was upregulated by mimics and downregulated by inhibitors (The top band of NUMB represents the mainly expressed protein isoform in 143B cells). I. The binding 3'UTR nucleotides and the mutation sequences of NUMB predicted by TargetScan were constructed into the luciferase reporter plasmid. J. The luciferase activity was markedly suppressed when co-transfected with miR146a-5p and wild-type reporter plasmid of NUMB in HEK-293T cells. K, L. Following the over-expression of circCRIM1, protein levels of NUMB raised, whereas NOTCH and Hes-1 decreased in both MNNG/HOS and 143B cells. M, N. Elevated expression levels of NUMB induced by circCRIM1 were attenuated after co-transfection with miR146a-5p, while down-regulation expressed NOTCH and Hes-1 were restored in the presence of miR146a-5p. Data are represented as mean ± SEM. $^*P < 0.05$, $^{**}P < 0.01$.

Subsequently, IHC staining of NUMB showed more brown precipitates in the cytoplasm and nucleus in the circCRIM1 overexpression group compared to the negative control group, while NOTCH and HES-1 showed stronger positive staining in the negative control group (**Figure 6G**, **6H**), which is consistent with the results obtained from our *in vitro* western blot experiments. Altogether, these data suggest antitumor effects of circCRIM1 *in vivo* (**Figure 6I**).

Discussion

In recent years, circRNAs have been shown to play essential roles in many physiological processes, especially in the malignant progression

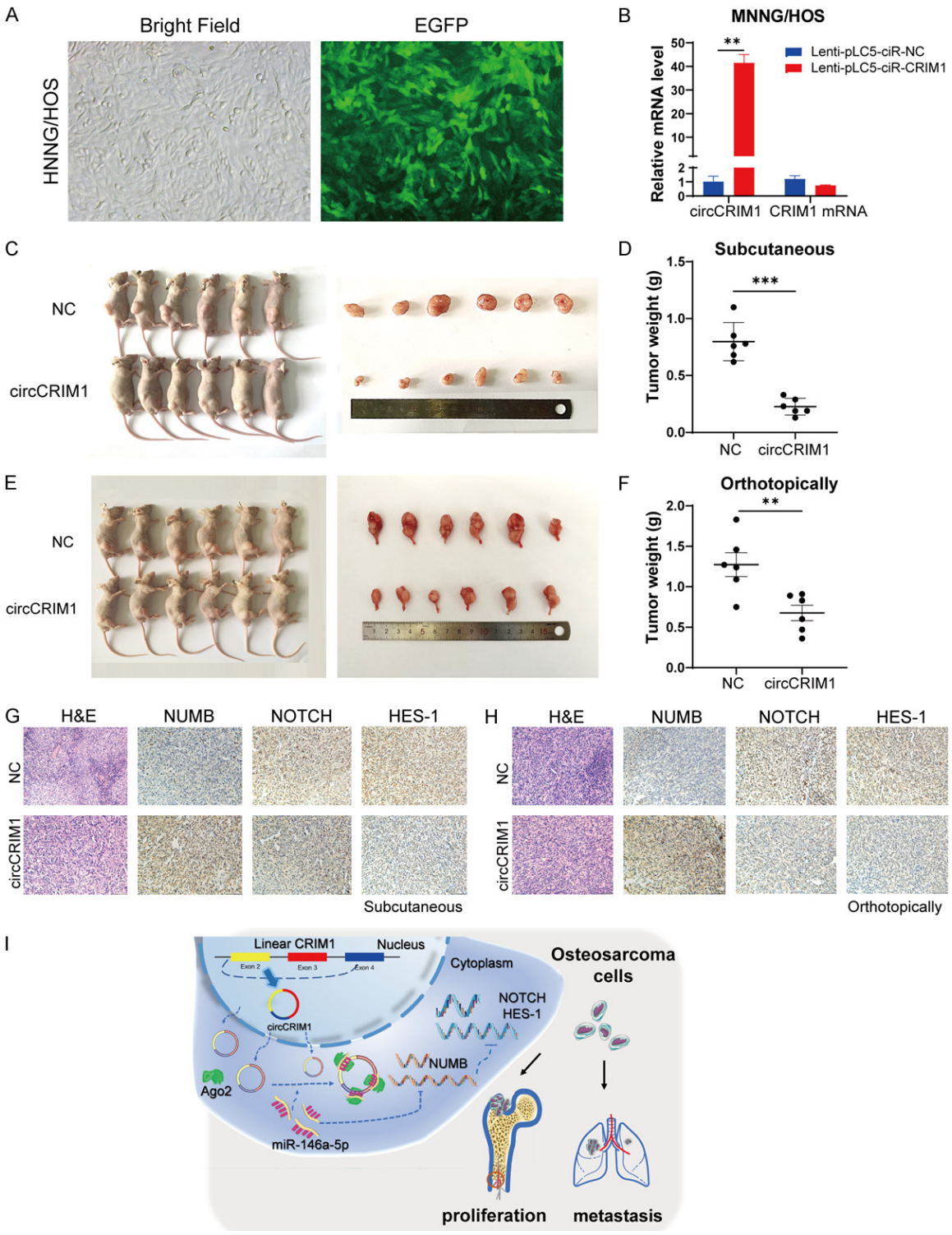

Figure 6. circCRIM1 inhibits the tumor growth of OS *in vivo*. (A) MNNG/HOS cells were infected with the lentivirus with an MOI value of 20, and the images are green fluorescent showing infection efficiency. As well as verifying the expression level of circCRIM1 in the stably transfected cell line with the RT-qPCR assay, circCRIM1 was elevated at a fold of 40, while there was no statistical difference in the level of CRIM1 mRNA change (B). (C, D) Representative images of xenograft tumors after subcutaneous injection of MNNG/HOS cells. Tumor volumes and weight were significantly reduced in the circCRIM1 overexpression group compared to the Negative Control group (n = 6 in each group). (E, F) The tumor tissue images of orthotopic injection of MNNG/HOS cells at the tibial plateau. The scatter plot showed that the tumor weight in the circCRIM1 group was significantly lower than that in the Negative Control group (n = 6 in each group). (G) Images show H&E staining and IHC staining of subcutaneous xenograft tumors. The

protein level of NUMB, NOTCH and HES-1 was assessed with IHC staining. The magnification of images was 200×. Scale bar = 100 μm. (H) The representative images present H&E and IHC staining of the orthotopic xenograft tumor slides. (I) The diagram of the circCRIM1/miR146a-5p/NUMB axis in osteosarcoma.

of tumors. Shang et al. reported a circRNF609-FMRP-RAC1 axis that was strongly associated with the metastasis of acral and cutaneous melanoma. circRNF609 might participate in regulation of the stability of RAC1 mRNA by binding to FMRP, which ultimately downregulated RAC1 mRNA and protein levels and inhibited the metastasis of melanoma cells [16].

circCRIM1 is derived from gene *CRIM1* and have been shown to be involved in oncogenesis of multiple malignancies, including nasopharyngeal carcinoma, lung adenocarcinoma, and hepatocellular carcinoma as well [20, 22, 23]. Interestingly, both oncogenic and tumor suppressive roles of circCRIM1 in OS have been reported recently. Wu et al. have detected low expression of circCRIM1 in OS cell lines and OS tissue samples, suggesting that circCRIM1 inhibits OS progression possibly by interacting with miR-513 [25]. However, circCRIM1l was reportedly upregulated in some of the OS cell lines and plays an oncogenic role in OS development, possibly via regulation of the miR-432-5p/HDAC4 axis [25]. We notice that by searching the circRNA database, there exist 107 circRNAs produced by cyclization of the *CRIM1* gene, including circCRIM1 (circ_0002346). circ_0053958 is also one of the circRNAs derived from the cyclization of the host gene *CRIM1* mRNA. Although circRNAs cyclizing with the host gene may get the same circRNA ID, their length, location on the chromosome, and the ways they function are completely different [42, 43].

To clarify the role of circCRIM1 in OS development, we examined its expression in four OS cell lines and detected decreased expression of cirCRIM1, which is in agreement with previous results as reported by Wu et al. [42]. To determine its *in vitro* function on OS cells, we showed that overexpression of circCRIM1 in OS cells significantly suppressed the proliferation, migration, and invasive ability of OS cells, suggesting its tumor suppressive role of circCRIM1 in OS. Through a series of bioinformatics predictions and the dual-luciferase reporter assay, we detected direct binding between miR146a-5p and circCRIM1. RT-qPCR and FISH analyses also confirmed the high binding capacity of miR146a-5p on circCRIM1. Moreover, we found that overexpression of miR146a-5p in rescue experiments mitigated the inhibitory effect of circCRIM1 on the malignancy of OS cells, suggesting that circRNA may show its antitumor effects in OS by acting as a sponge for miRNA.

Previous studies have revealed that miR146a-5p is differentially expressed and may play an oncogenic or tumor suppressive role in multiple tumors [38, 44, 45]. MiR146a-5p was reported to suppress the energy metabolism and tumor growth by targeting CD147 in anaplastic large cell lymphoma (ALCL) [46]. miR146a-5p may alleviate the deterioration of colitis via inhibiting SUMO1 expression and its binding to β-catenin [47]. Furthermore, miR-146a is involved in the angiogenic of endothelial cells in hepatocellular carcinoma by promoting the expression of platelet-derived growth factor receptor α (PDGFRA) [48]. In this study, we confirmed that miR146a-5p was up-regulated in OS cell lines, and that miR146a-5p may cause decreased expression of NUMB, a downstream target and a novel mechanism proposed for OS. NUMB has been essential for cell fate determination such as asymmetric cell division and cell fate choice, endocytosis, cell adhesion, and cell migration, and thus tumorigenesis. We have also demonstrated that the expression of NUMB, as a downstream target of miR146a-5p was positively regulated by circCRIM1. To further determine the effect and mechanism of circCRIM1 on OS, we evaluated the correlation of Notch signaling, the classical regulatory target of NUMB gene. Our results support that overexpression of circCRIM1 inhibited miR146a-5p levels and positively promoted the activity of NUMB, which in turn inhibited Notch1 and Hes1 both in *vitro* and in *vivo*.

CircCRIM1, a circular RNA molecule, has shown promising potential in various applications related to osteosarcoma and other tumor types. Its role as a suppressor of OS progression through sponging miR146a-5p and targeting NUMB has significant implications in cancer research. Furthermore, circCRIM1's unique circular structure and stability make it an attrac-

tive candidate for diagnostic and prognostic biomarkers in OS. It holds promise as a non-invasive biomarker for early detection, monitoring disease progression, and assessing treatment response. Additionally, the regulatory functions of circCRIM1 in cancer-related pathways suggest its therapeutic potential. Future research may unveil additional applications of circCRIM1 in cancer biology and pave the way for personalized treatment strategies.

Conclusions

Our study revealed the new light on the significance of circCRIM1 in OS progression. We have shown that forced overexpression of circCRIM1 suppresses the proliferation and migration ability as well as the cell viability of OS cells in *vitro* and tumor growth both in situ and in subcutaneous tumor models. Mechanically, circCRIM1 inhibits the progression of OS by acting as a sponge for miR146a-5P, which in turn promotes the expression of downstream target gene NUMB and inhibits NOTCH signaling. circCRIM1 might serve as a novel regulator of the miR46a-5p/NUMB axis and provide a novel theoretical basis contributes to the diagnosis and therapeutics of OS.

Acknowledgements

This study was supported in part by grants from the Jiangsu provincial key research and development program (#BE2020679 to Q.Z.).

Disclosure of conflict of interest

None.

Abbreviations

OS, Osteosarcoma; circRNAs, Circular RNAs; CRIM1, cysteine rich transmembrane BMP regulator 1; DCM, Diabetic cardiomyopathy; VCP, valosin-containing protein; IL-6, Interleukin-6; TAMs, Tumor-associated macrophages; NPC, Nasopharyngeal carcinoma; NSCLC, Non-small cell lung cancer; FISH, Fluorescence in situ hybridization; DMEM, Dulbecco's Modified Eagle Medium; SiRNAs, Small interfering RNAs; MiR, MicroRNA; FBS, Fetal bovine serum; PVDF, Polyvinylidene fluoride; EdU, 5-ethynyl-2'-deoxyuridine; CCK-8, Cell Counting Kit-8; IHC, Histology and Immunohistochemistry; GEO, Gene expression omnibus; WT, Wild type; 3'UTR, 3' untranslational region; ALCL, Anaplastic large cell lymphoma; PDGFRA, Platelet-derived growth factor receptor α.

Address correspondence to: Dr. Qiping Zheng, Department of Hematological Laboratory Science, Jiangsu Key Laboratory of Medical Science and Laboratory Medicine, School of Medicine, Jiangsu University, Zhenjiang 212013, Jiangsu, China. E-mail: qp_zheng@hotmail.com

References

[1] Arndt CA and Crist WM. Common musculoskeletal tumors of childhood and adolescence. N Engl J Med 1999; 341: 342-352.

[2] Stiller CA, Craft AW and Corazziari I; EUROCARE Working Group. Survival of children with bone sarcoma in Europe since 1978: results from the EUROCARE study. Eur J Cancer 2001; 37: 760-766.

[3] Meltzer PS and Helman LJ. New horizons in the treatment of osteosarcoma. N Engl J Med 2021; 385: 2066-2076.

[4] Bacci G, Bertoni F, Longhi A, Ferrari S, Forni C, Biagini R, Bacchini P, Donati D, Manfrini M, Bernini G and Lari S. Neoadjuvant chemotherapy for high-grade central osteosarcoma of the extremity. Histologic response to preoperative chemotherapy correlates with histologic subtype of the tumor. Cancer 2003; 97: 3068-3075.

[5] Bernthal NM, Federman N, Eilber FR, Nelson SD, Eckardt JJ, Eilber FC and Tap WD. Long-term results (> 25 years) of a randomized, prospective clinical trial evaluating chemotherapy in patients with high-grade, operable osteosarcoma. Cancer 2012; 118: 5888-5893.

[6] Kager L, Zoubek A, Pötschger U, Kastner U, Flege S, Kempf-Bielack B, Branscheid D, Kotz R, Salzer-Kuntschik M, Winkelmann W, Jundt G, Kabisch H, Reichardt P, Jürgens H, Gadner H and Bielack SS; Cooperative German-Austrian-Swiss Osteosarcoma Study Group. Primary metastatic osteosarcoma: presentation and outcome of patients treated on neoadjuvant Cooperative Osteosarcoma Study Group protocols. J Clin Oncol 2003; 21: 2011-2018.

[7] Longhi A, Fabbri N, Donati D, Capanna R, Briccoli A, Biagini R, Bernini G, Ferrari S, Versari M and Bacci G. Neoadjuvant chemotherapy for patients with synchronous multifocal osteosarcoma: results in eleven cases. J Chemother 2001; 13: 324-330.

[8] Harris MA and Hawkins CJ. Recent and ongoing research into metastatic osteosarcoma treatments. Int J Mol Sci 2022; 23: 3817.

[9] Siegel RL, Miller KD, Fuchs HE and Jemal A. Cancer Statistics, 2021. CA Cancer J Clin 2021; 71: 7-33.

[10] Li B, Xi W, Bai Y, Liu X, Zhang Y, Li L, Bian L, Liu C, Tang Y, Shen L, Yang L, Gu X, Xie J, Zhou Z, Wang Y, Yu X, Wang J, Chao J, Han B and Yao H. FTO-dependent m(6)A modification of Plpp3 in circSCMH1-regulated vascular repair and functional recovery following stroke. Nat Commun 2023; 14: 489.

[11] Yuan Q, Sun Y, Yang F, Yan D, Shen M, Jin Z, Zhan L, Liu G, Yang L, Zhou Q, Yu Z, Zhou X, Yu Y, Xu Y, Wu Q, Luo J, Hu X and Zhang C. CircRNA DICAR as a novel endogenous regulator for diabetic cardiomyopathy and diabetic pyroptosis of cardiomyocytes. Signal Transduct Target Ther 2023; 8: 99.

[12] Vo JN, Cieslik M, Zhang Y, Shukla S, Xiao L, Zhang Y, Wu YM, Dhanasekaran SM, Engelke CG, Cao X, Robinson DR, Nesvizhskii AI and Chinnaiyan AM. The landscape of circular RNA in cancer. Cell 2019; 176: 869-881, e13.

[13] Li J, Sun D, Pu W, Wang J and Peng Y. Circular RNAs in cancer: biogenesis, function, and clinical significance. Trends Cancer 2020; 6: 319-336.

[14] Yang Q, Li F, He AT and Yang BB. Circular RNAs: expression, localization, and therapeutic potentials. Mol Ther 2021; 29: 1683-1702.

[15] Yalamarty SSK, Filipczak N, Khan MM and Torchilin VP. Role of circular RNA and its delivery strategies to cancer - an overview. J Control Release 2023; 356: 306-315.

[16] Shang Q, Du H, Wu X, Guo Q, Zhang F, Gong Z, Jiao T, Guo J and Kong Y. FMRP ligand circZNF609 destabilizes RAC1 mRNA to reduce metastasis in acral melanoma and cutaneous melanoma. J Exp Clin Cancer Res 2022; 41: 170.

[17] Zhou B, Mo Z, Lai G, Chen X, Li R, Wu R, Zhu J and Zheng F. Targeting tumor exosomal circular RNA cSERPINE2 suppresses breast cancer progression by modulating MALT1-NF-κB-IL-6 axis of tumor-associated macrophages. J Exp Clin Cancer Res 2023; 42: 48.

[18] Ghafouri-Fard S, Dinger ME, Maleki P, Taheri M and Hajiesmaeili M. Emerging role of circular RNAs in the pathobiology of lung cancer. Biomed Pharmacother 2021; 141: 111805.

[19] Zhao L, Chen R, Qiu J, Huang Y, Lian C, Zhu X, Cui J, Wang S, Wang S, Hu Z and Wang J. CircCRIM1 ameliorates endothelial cell angiogenesis in aging through the miR-455-3p/Twist1/VEGFR2 signaling axis. Oxid Med Cell Longev 2022; 2022: 2062885.

[20] Ji Y, Yang S, Yan X, Zhu L, Yang W, Yang X, Yu F, Shi L, Zhu X, Lu Y, Zhang C, Lu H and Zhang F. CircCRIM1 promotes hepatocellular carcinoma proliferation and angiogenesis by sponging miR-378a-3p and regulating SKP2 expression. Front Cell Dev Biol 2021; 9: 796686.

[21] Du Y, Liu X, Zhang S, Chen S, Guan X, Li Q, Chen X and Zhao Y. CircCRIM1 promotes ovarian cancer progression by working as ceRNAs of CRIM1 and targeting miR-383-5p/ZEB2 axis. Reprod Biol Endocrinol 2021; 19: 176.

[22] Wang L, Liang Y, Mao Q, Xia W, Chen B, Shen H, Xu L, Jiang F and Dong G. Circular RNA circCRIM1 inhibits invasion and metastasis in lung adenocarcinoma through the microRNA (miR)-182/miR-93-leukemia inhibitory factor receptor pathway. Cancer Sci 2019; 110: 2960-2972.

[23] Hong X, Liu N, Liang Y, He Q, Yang X, Lei Y, Zhang P, Zhao Y, He S, Wang Y, Li J, Li Q, Ma J and Li Y. Circular RNA CRIM1 functions as a ceRNA to promote nasopharyngeal carcinoma metastasis and docetaxel chemoresistance through upregulating FOXQ1. Mol Cancer 2020; 19: 33.

[24] Peng W, Ye L, Xue Q, Wei X, Wang Z, Xiang X, Zhang S, Zhang P, Wang H and Zhou Q. Silencing of circCRIM1 drives IGF2BP1-mediated NSCLC immune evasion. Cells 2023; 12: 273.

[25] Wu P, Kong Y, Dai Z, Liu W and Zhao Z. The circular RNA circCRIM1 inhibits osteosarcoma progression through sponging miR-513. Mamm Genome 2021; 32: 495-502.

[26] Liu J, Feng G, Li Z, Li R and Xia P. Knockdown of CircCRIM1 inhibits HDAC4 to impede osteosarcoma proliferation, migration, and invasion and facilitate autophagy by targeting miR-432-5p. Cancer Manag Res 2020; 12: 10199-10210.

[27] Liu W, Zhang J, Zou C, Xie X, Wang Y, Wang B, Zhao Z, Tu J, Wang X, Li H, Shen J and Yin J. Microarray expression profile and functional analysis of circular RNAs in osteosarcoma. Cell Physiol Biochem 2017; 43: 969-985.

[28] Jeck WR and Sharpless NE. Detecting and characterizing circular RNAs. Nat Biotechnol 2014; 32: 453-461.

[29] Guo JU, Agarwal V, Guo H and Bartel DP. Expanded identification and characterization of mammalian circular RNAs. Genome Biol 2014; 15: 409.

[30] Hansen TB, Jensen TI, Clausen BH, Bramsen JB, Finsen B, Damgaard CK and Kjems J. Natural RNA circles function as efficient microRNA sponges. Nature 2013; 495: 384-388.

[31] Memczak S, Jens M, Elefsinioti A, Torti F, Krueger J, Rybak A, Maier L, Mackowiak SD, Gregersen LH, Munschauer M, Loewer A, Ziebold U, Landthaler M, Kocks C, le Noble F and Rajewsky N. Circular RNAs are a large class of animal RNAs with regulatory potency. Nature 2013; 495: 333-338.

[32] Kristensen LS, Andersen MS, Stagsted LVW, Ebbesen KK, Hansen TB and Kjems J. The bio-

genesis, biology and characterization of circular RNAs. Nat Rev Genet 2019; 20: 675-691.
[33] Krüger J and Rehmsmeier M. RNAhybrid: microRNA target prediction easy, fast and flexible. Nucleic Acids Res 2006; 34: W451-454.
[34] John B, Enright AJ, Aravin A, Tuschl T, Sander C and Marks DS. Human MicroRNA targets. PLoS Biol 2004; 2: e363.
[35] Lewis BP, Shih IH, Jones-Rhoades MW, Bartel DP and Burge CB. Prediction of mammalian microRNA targets. Cell 2003; 115: 787-798.
[36] Li JH, Liu S, Zhou H, Qu LH and Yang JH. starBase v2.0: decoding miRNA-ceRNA, miRNA-ncRNA and protein-RNA interaction networks from large-scale CLIP-Seq data. Nucleic Acids Res 2014; 42: D92-97.
[37] Garo LP, Ajay AK, Fujiwara M, Gabriely G, Raheja R, Kuhn C, Kenyon B, Skillin N, Kadowaki-Saga R, Saxena S and Murugaiyan G. MicroRNA-146a limits tumorigenic inflammation in colorectal cancer. Nat Commun 2021; 12: 2419.
[38] Shahriar A, Ghaleh-Aziz Shiva G, Ghader B, Farhad J, Hosein A and Parsa H. The dual role of mir-146a in metastasis and disease progression. Biomed Pharmacother 2020; 126: 110099.
[39] Hamberg M, Backes C, Fehlmann T, Hart M, Meder B, Meese E and Keller A. MiRTargetLink-miRNAs, genes and interaction networks. Int J Mol Sci 2016; 17: 564.
[40] Kehl T, Kern F, Backes C, Fehlmann T, Stöckel D, Meese E, Lenhof HP and Keller A. miRPathDB 2.0: a novel release of the miRNA pathway dictionary database. Nucleic Acids Res 2020; 48: D142-D147.
[41] Giuli MV, Giuliani E, Screpanti I, Bellavia D and Checquolo S. Notch signaling activation as a hallmark for triple-negative breast cancer subtype. J Oncol 2019; 2019: 8707053.
[42] Wu Y, Xie Z, Chen J, Chen J, Ni W, Ma Y, Huang K, Wang G, Wang J, Ma J, Shen S and Fan S. Circular RNA circTADA2A promotes osteosarcoma progression and metastasis by sponging miR-203a-3p and regulating CREB3 expression. Mol Cancer 2019; 18: 73.
[43] Xu JZ, Shao CC, Wang XJ, Zhao X, Chen JQ, Ouyang YX, Feng J, Zhang F, Huang WH, Ying Q, Chen CF, Wei XL, Dong HY, Zhang GJ and Chen M. circTADA2As suppress breast cancer progression and metastasis via targeting miR-203a-3p/SOCS3 axis. Cell Death Dis 2019; 10: 175.
[44] Wang H, Zhang S, Li T, Wang L, Lv W, Wang S, Ma D, Zang Y, Zhu X, Xu Y, Zheng L, Shen J and Wei W. MicroRNA-146a promotes proliferation, migration, and invasion of HepG2 via regulating FLAP. Cancer Cell Int 2022; 22: 149.
[45] Simanovich E, Brod V, Rahat MM and Rahat MA. Function of miR-146a-5p in tumor cells as a regulatory switch between cell death and angiogenesis: macrophage therapy revisited. Front Immunol 2018; 8: 1931.
[46] Montes-Mojarro IA, Steinhilber J, Griessinger CM, Rau A, Gersmann AK, Kohlhofer U, Fallier-Becker P, Liang HC, Hofmann U, Haag M, Klapper W, Schaeffeler E, Pichler BJ, Schwab M, Fend F, Bonzheim I and Quintanilla-Martinez L. CD147 a direct target of miR-146a supports energy metabolism and promotes tumor growth in ALK+ ALCL. Leukemia 2022; 36: 2050-2063.
[47] Wang J, Pei B, Yan J, Xu X, Fang AN, Ocansey DKW, Zhang X, Qian H, Xu W and Mao F. hucMSC-derived exosomes alleviate the deterioration of colitis via the miR-146a/SUMO1 axis. Mol Pharm 2022; 19: 484-493.
[48] Zhu K, Pan Q, Zhang X, Kong LQ, Fan J, Dai Z, Wang L, Yang XR, Hu J, Wan JL, Zhao YM, Tao ZH, Chai ZT, Zeng HY, Tang ZY, Sun HC and Zhou J. MiR-146a enhances angiogenic activity of endothelial cells in hepatocellular carcinoma by promoting PDGFRA expression. Carcinogenesis 2013; 34: 2071-2079.

Supplementary Material 1

Codes:

```
library(data.table)
a=fread('Gse96964probeMatrix.txt',data.table = F)
a[1:4,1:4]
b=read.table('ann.txt',sep = '\t',header = T)
tail(head(b,20))
d=merge(a,b,by.x='ID_REF',by.y='circBase ID cross-references')
e=read.table('circBase ID cross-references.txt',header = T)
head(e)
f=merge(e,d,by='circRNA')
head(f[,1:6])
```